Theory of high-field magnetotransport in a percolating medium

Andrey K. Sarychev
Institute for High Temperature of the Russian Academy of Sciences, Moscow, Russia and School of Physics and Astronomy, Raymond and Beverly Sackler Faculty of Exact Sciences, Tel Aviv University, Tel Aviv 69978, Israel*

David J. Bergman and Yakov M. Strelniker
School of Physics and Astronomy, Raymond and Beverly Sackler Faculty of Exact Sciences, Tel Aviv University, Tel Aviv 69978, Israel

(Received 29 May 1992; revised manuscript received 18 January 1993)

The critical behavior of magnetotransport in a percolating medium in the presence of a magnetic field H of arbitrary strength is discussed. A discrete network model is used to solve the problem exactly for a three-dimensional Sierpinski-gasket fractal, and to perform a direct Monte Carlo simulation of a percolating medium. A very efficient algorithm is used to calculate transport properties in the vicinity of the percolation threshold. We find that there is strong magnetoresistance near the percolation threshold. We also find a different scaling behavior of the effective Ohmic resistivity $\rho^{(e)}(p,H)$ and Hall coefficient $R_H^{(e)}(p,H)$ as functions of the concentration p and magnetic field H. This scaling is due to the appearance of a field-dependent length—the magnetic correlation length ξ_H. In a percolating metal-insulator mixture, the resistivity ratio with and without a field $\rho^{(e)}(p,H)/\rho^{(e)}(p,0)$ is predicted to saturate as $p \to p_c$ at a value that is proportional to $H^{3.1}$.

I. INTRODUCTION

In spite of the considerable effort devoted by theorists during the last 15 years to the study of percolating systems, relatively little work has been done on electrical conduction in the presence of a magnetic field, and almost all of that was restricted to weak magnetic fields.[1–9] On the other hand, it is well known that the investigation of transport properties in metals and semiconductors in the presence of a strong magnetic field is an important tool for understanding the microscopic structure of such materials (see, e.g., Ref. 10). It is reasonable to expect that transport in the presence of a strong magnetic field will play a similar role in the case of percolating systems. In this paper we consider the transport properties of three-dimensional (3D), percolating composite media, consisting of metal and dielectric particles, in the presence of a strong magnetic field.

In the case of 2D composite media, the duality transformation has been used to obtain some exact results.[11–14] It was proven that the ohmic resistance does not depend on the magnetic field and that the Hall coefficient is a constant for any concentration p of the conducting component above the percolation threshold p_c. The theoretical investigation of 3D percolating composites in a strong magnetic field has been restricted to some heuristic arguments,[15] applications of the effective medium theory (EMT),[15–17] and a real-space renormalization-group transformation that was a precursor to the study reported here.[18] From EMT it follows that, in the case of metals with a closed Fermi surface, both the transverse and the longitudinal magnetoresistance are linear in the magnetic field for strong fields, whereas the Hall coefficient is only weakly dependent on that field. The slope of the (linear) magnetoresistance tends to zero when the volume fraction of metal p approaches the percolation threshold p_c. Thus the diagonal terms of the resistivity tensor become independent of the magnetic field at the percolation threshold.

This last result of EMT is in obvious contradiction with results for the magnetoresistance of the simple configurations of 3D percolation channels shown in Fig. 1. Suppose that the conducting component has no intrinsic magnetoresistance, i.e., its ohmic resistivity ρ does not depend on the magnetic field. Then the thin, singly connected channel in Fig. 1(a) has no magnetoresistance. The sit-

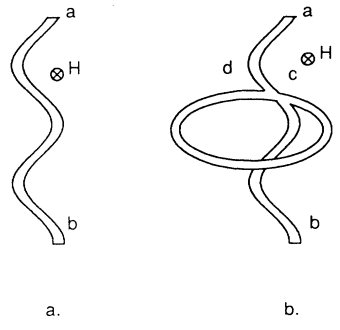

FIG. 1. (a) Singly connected percolation channel with resistance R. (b) The same channel but with an extra loop attached at one point. The resistance between the points a and b now depends on the magnetic field component in the plane of the loop and is much greater than R.

uation is quite different in the case of the channel with a transverse loop [Fig. 1(b)]: In the absence of a magnetic field, the loop has almost no effect upon the resistance $R'(0)$ between the end points a, b, so that $R'(0) \approx R$. But when a strong magnetic field is present, the Hall resistivity ρ_H can be much larger than the ohmic resistivity, $\rho_H/\rho \equiv H \gg 1$. A unit current flowing in the channel ab then induces a large Hall emf in the loop cd. This produces a large ohmic current $\sim H$ in the loop, and that, in turn, induces an even larger Hall voltage $\sim H^2$ in the ab channel. Thus a large magnetoresistance, which is quadratic in H, results from going to second order in the Hall effect, and we get $R'(H)/R'(0) \sim H^2$. From this example we conclude that some of the percolation channels have their resistance changed substantially in a strong magnetic field. The importance of these configurations is hard to judge quantitatively, but their existence leads us to treat with suspicion the EMT prediction that there is no magnetoresistance at p_c. Another reason for questioning the results of EMT, even far away from the percolation threshold p_c, is the fact, entirely ignored by EMT, that the scale of the (electric) field and current distortions increases by a factor $H \gg 1$ in a strong magnetic field.[19,20]

In this paper we report on a detailed study of the effective magnetoresistivity $\rho^{(e)}$ and Hall coefficient $R_H^{(e)}$ in percolating composites. We use a simple, exactly solvable regular fractal model, based on the 3D Sierpinski gasket, as well as some direct Monte Carlo (MC) simulations, to show that a different type of scaling behavior appears in the system in a strong magnetic field. This scaling is a consequence of the presence of an additional characteristic length, the magnetic correlation length ξ_H, which depends on the magnetic field H. In contrast with the predictions of EMT, we find that there is a strong magnetoresistance near the percolation threshold, which saturates as the field tends to infinity.

The rest of the paper is organized as follows. In Sec. II we describe a lumped circuit element that is a discrete model for an isotropic conductor in the presence of an arbitrarily strong magnetic field. This model allows us to apply a number of standard approaches for studying the critical behavior near a percolation threshold, all based upon discrete network models (see, e.g., Ref. 21). In Sec. III we consider the 3D Sierpinski gasket as a model for the backbone of the percolating cluster (see Ref. 22), with one of the above-mentioned circuit elements placed at each vertex. The bulk effective resistivity tensor $\rho^{(e)}$ for this system is calculated exactly as function of the linear size L and the strength of the magnetic field H. Even though this fractal is accurately self-similar, it is shown that the current distribution is quite different when $L \ll \xi_H$ and when $L \gg \xi_H$, where ξ_H is an appropriately defined magnetic correlation length. This crossover leads to scaling behavior of the resistivity as function of L/ξ_H. In Sec. IV we present the results of Monte Carlo simulations of random networks made of the above-mentioned circuit elements. An efficient algorithm is used to calculate the resistivity tensor for such networks in the vicinity of the percolation threshold. The ohmic and Hall resistivities again exhibit new scaling behavior in the presence of a strong magnetic field. This behavior is consistent with what was found for the Sierpinski-gasket model. Section V is a summary and some conclusions. In the Appendix we provide some technical details of the Sierpinski-gasket calculations and discuss the effects of different types of boundary conditions on the results of the numerical simulations.

II. DISCRETE CIRCUIT ELEMENT FOR MODELING MAGNETOTRANSPORT

The continuum material we wish to represent has a resistivity tensor $\hat{\rho}$ with elements given by

$$\hat{\rho} = \begin{pmatrix} \rho & -\rho_H & 0 \\ \rho_H & \rho & 0 \\ 0 & 0 & \rho \end{pmatrix}, \tag{1}$$

where the ohmic resistivity ρ is independent of the magnetic field H and the Hall resistivity ρ_H is proportional H. This represents an isotropic, free-electron metal with a magnetic field in the z direction, and no intrinsic magnetoresistance. Using dimensionless units for H, we can write $H \equiv \rho_H/\rho = \omega_L \tau$, where the Larmor frequency is given by $\omega_L = e\mathcal{H}/mc$. Here $\mathcal{H}$ is the magnetic field in conventional units and τ is the conductivity relaxation time.

In spite of the rather specific assumptions made here, our main results are valid for any material in which the ohmic resistivity ρ saturates and the Hall resistivity ρ_H is proportional to H when $H \to \infty$. That is the case in metal-insulator composites where the conducting component is an uncompensated metal with a closed Fermi surface or a semiconductor.

Finding a discrete circuit element (DCE) to represent $\hat{\rho}$ is a nontrivial problem, as can be seen from the fact that at least one seemingly obvious model turned out to lead to random networks that were in a different universality class of critical properties from that of real, percolating, continuum composites.[4,7] Our DCE has six external terminals (legs), one along each ray of the coordinate axes [see Fig. 2(a)], at which potentials V_i are applied and electric currents I_j flow. The relations between the currents and the potentials in such a DCE are characterized by a 6×6 resistance matrix $\hat{R}$,

$$R_{ij} \equiv \frac{1}{2}(\rho\delta_{ij} + \rho_H Y_{ij}), \tag{2}$$

where the antisymmetric matrix $\hat{Y}$ is given by

$$\hat{Y} = \begin{pmatrix} 0 & -1 & 0 & 1 & 0 & 0 \\ 1 & 0 & -1 & 0 & 0 & 0 \\ 0 & 1 & 0 & -1 & 0 & 0 \\ -1 & 0 & 1 & 0 & 0 & 0 \\ 0 & 0 & 0 & 0 & 0 & 0 \\ 0 & 0 & 0 & 0 & 0 & 0 \end{pmatrix}, \tag{3}$$

and where ρ and ρ_H are the same as in (1). When $H = 0$,

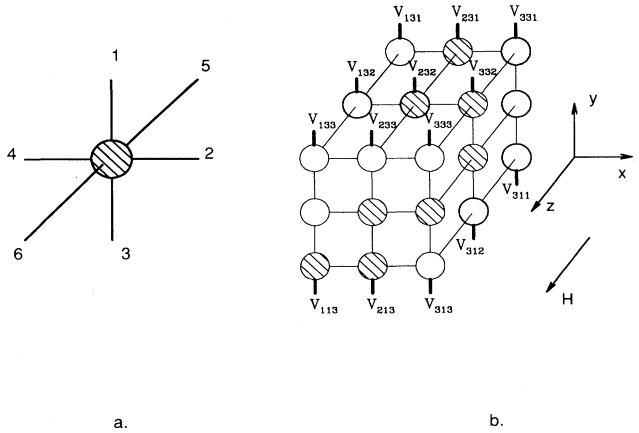

FIG. 2. (a) The basic discrete circuit element (DCE) which mimics the magnetotransport properties of a real continuum material. The numbering of the terminals or legs corresponds to the rows and columns of the resistance matrix $\hat{R}$ of (2). (b) Portion of a simple cubic network of the basic DCE's. Hatched circles denote the presence of a DCE, while empty circles denote its absence. External potentials $V_{i,j,k}$ are applied to the terminals at the top and bottom layers.

ρ_H vanishes, and this DCE is equivalent to six identical ohmic resistors connected at one point [see Fig. 2(a)]. When $H \neq 0$, ρ_H does not vanish, and this DCE then has an antisymmetric part. Therefore a current flowing along the x axis induces a voltage along the y axis, and vice versa. This model is equivalent to the one used earlier by Straley in connection with the low-field Hall effect,[9] but is represented in a different way. In our representation of this model, the potentials at the six terminals are required to add up to zero. As a result of this, the potential scales of different DCE's are shifted with respect to each other. This causes no difficulty since Kirchhoff's equations can be written entirely in terms of potential differences on each DCE. In this model, a component of the local electric field is represented by the voltage difference between a pair of terminals on the same DCE, and a component of the local current density is represented by the current flowing through one of the inter-DCE connection points.

A uniform conducting medium is represented by placing these DCE's at all the sites of a simple cubic lattice and connecting together each pair of adjacent terminals from neighboring DCE's at the center of the appropriate network bond [see Fig. 2(b)]. If uniform boundary conditions are applied to the voltages at the external terminals of such a network, the resulting current distribution (or current density) will also be uniform, and the resistivity matrix which describes the relation between them will be simply $\hat{\rho}$ of (1). A 3D random, metal-insulator composite with a metallic volume fraction p will be represented by a similar network in which the individual DCE's are chosen at random to be either metallic (with probability p), or insulating (with probability $1-p$).

The 2D version of this model, for the case where H is perpendicular to the sample plane, is easily seen to be a four-terminal DCE which is described by a 4×4 resistivity matrix that is the upper left part of $\hat{R}$ of (2). A uniform square network of these elements is a good model for magnetotransport in a 2D metal. That a random square network of such elements provides a good model for a 2D random, metal-insulator composite is ensured by the fact that there exists an exact duality transformation for this system (see Ref. 18).

III. EXACT SOLUTION FOR MAGNETOTRANSPORT IN A 3D SIERPINSKI-GASKET MODEL

We are interested in the bulk effective conductivity tensor of a percolating composite. In the case of a metal-insulator composite, it is the backbone of the percolating cluster that determines the transport properties.[21] When a magnetic field is applied to the system, the contribution of different parts of the backbone to the total resistivity changes. For example, when $H = 0$, closed loops attached to the backbone at a single site do not carry any current and hence make no contribution to the transport. In contrast, when H is nonzero and large, they can have a huge effect on the transport (see Fig. 1). Therefore it is not clear that a model of the backbone that reproduces well the transport properties at $H = 0$ will also work well for nonzero H. With this proviso in mind, we nevertheless use the well-known Sierpinski-gasket model for the backbone, originally proposed for a system with no magnetic field.[22] The first three stages of iteration of the 3D Sierpinski gasket are shown in Fig. 3. In order to study magnetotransport, we place a four-terminal DCE, like the ones used to simulate a 2D conductor in the previous section, at each vertex of the gasket. Because of the way the different DCE's are connected together, the entire structure is three dimensional and the best way to think of each DCE is as if it were a tetrahedron. This model was first introduced in Ref. 23. There we implicitly and erroneously assumed that the longitudinal and the transverse ohmic resistances are equal in all iterations. Therefore the results for the scaling behavior found in Ref. 23 are quantitatively wrong. Nevertheless they are

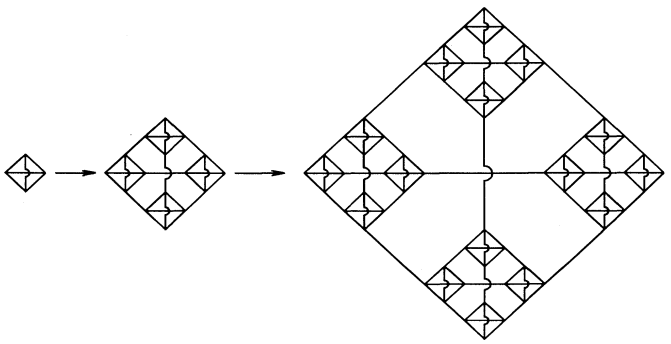

FIG. 3. Three initial stages or generations of the 3D Sierpinski-gasket fractal. By iterating this construction procedure it is possible to make a fractal of arbitrarily large linear size L.

similar to what we find here, and the qualitative conclusions are the same.

A tetrahedron with four terminals at its vertices, which characterizes the overall topology of the 3D gasket, is the minimal discrete object which can represent a continuum, 3D conducting medium in the presence of a magnetic field of arbitrary direction. The crucial fact which makes this possible is that we can simulate a current vector of arbitrary magnitude and direction, as well as an electric field of arbitrary magnitude and direction, by assigning appropriate values to the currents and voltages at the four terminals. For example, a current I flowing in a perpendicular direction into the page in Fig. 4 is represented by taking $I_{\rm I} = I_{\rm III} = I/2$, $I_{\rm II} = I_{\rm IV} = -I/2$. Similarly, a field E pointing in the same direction is represented by taking $V_{\rm I} = V_{\rm III} = E/2$, $V_{\rm II} = V_{\rm IV} = -E/2$.

A magnetic field of arbitrary magnitude and direction can be included in this description by considering its effect on the relationship between the electric field and current vectors of the DCE. The resistance matrix $\hat{R}$ of a single DCE obtained in this way can also be obtained from (2) by eliminating the last two rows and columns. In this way we get

$$R_{ij} = \frac{1}{2} R_0(\delta_{ij} + H_0 Y_{ij}), \tag{4}$$

where the antisymmetric matrix $\hat{Y}$ is given by

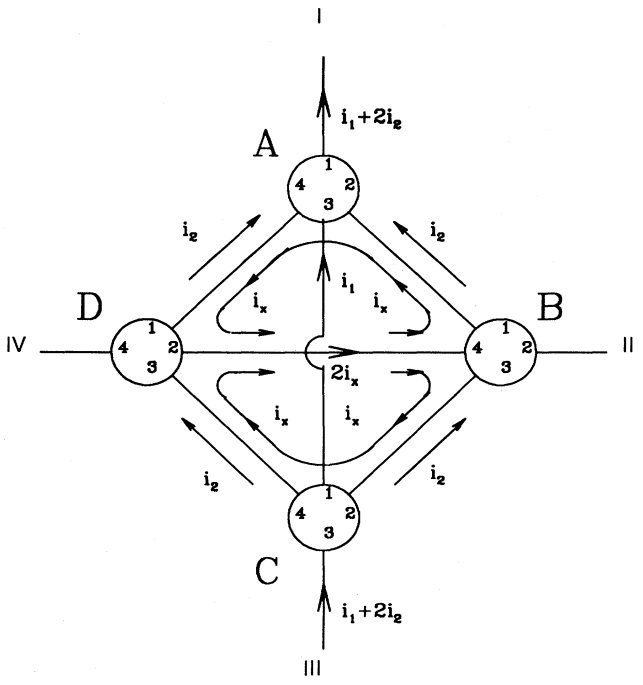

FIG. 4. Detailed scheme for the coupling of four four-terminal DCE's to create the first generation 3D Sierpinski gasket. In order to set up Kirchhoff's equations for the case where external current flows only into the external terminals I and III, three independent currents are introduced: i_1, i_2, and the loop current i_x, which is nonzero only when $H \neq 0$. The direction of H is perpendicular to the page.

$$\hat{Y} = \begin{pmatrix} 0 & -1 & 0 & 1 \\ 1 & 0 & -1 & 0 \\ 0 & 1 & 0 & -1 \\ -1 & 0 & 1 & 0 \end{pmatrix}. \tag{5}$$

Figure 4 shows the details of how four DCE's are connected up to create the first generation fractal, which also has four external terminals, in the case where H is perpendicular to the plane of the drawing. We start with DCE's which represent a free-electron metal and have the same resistance along the magnetic field and perpendicular to it. In the presence of a magnetic field this is no longer true for the gasket. For this reason the first generation fractal must be described by a matrix that is different in form from $\hat{R}$ of (4). The new matrix $\hat{R}$ depends upon three parameters $R_1 = \gamma R_3$, R_3, and H [see (A1) in the Appendix], where R_3 is the resistance along the magnetic field, R_1 is the resistance perpendicular to it, and HR_3 is the Hall resistance.

In the next stage, four of these first generation gaskets are connected together in the same way to make the second generation fractal, etc. The nth generation fractal thus has a linear size $L = 2^n$ and a resistance matrix of form (A1) with the parameters $R_1(R_0, H_0, L) = \gamma(H_0, L) R_3(R_0, H_0, L)$, $R_3(R_0, H_0, L)$, and $H(R_0, H_0, L)$. The transformation from the n to the $n+1$ generation fractal, which is an exact renormalization-group transformation, is found by solving Kirchhoff's equations (see the Appendix for details). This yields

$$R_3(n+1) = R_3 \frac{2 + \gamma(n)}{2}, \tag{6}$$

$$\gamma(n+1) = 2 \frac{[\gamma(n)+1]\{\gamma(n)[\gamma(n)+2] + H^2(n)\}}{[\gamma(n)+2]\{[\gamma(n)+1]^2 + H^2(n)\}} \tag{7}$$

$$H(n+1) = 2 \frac{\gamma(n)[\gamma(n)+2] + H^2(n)}{[\gamma(n)+2]\{[\gamma(n)+1]^2 + H^2(n)\}} H(n), \tag{8}$$

which can be iterated as many times as necessary to reach the final size $L = 2^n$. The initial values for the parameters are determined by the form of the original DCE resistance matrix. In the particular case of (4) those are $R_3(0) = R_1(0) = R_0$, $\gamma(0) = 1$ and $H(0) = H_0$.

It is easy to show that the values $H = 0$, $\gamma = 1$ constitute a stable fixed point of the transformation. For $|H_0| \ll 1$ the transverse ohmic resistivity $\rho_\perp \equiv 2a_0 L R_1(R_0, H_0, L)$ is equal (up to terms proportional to H_0^2) to the longitudinal ohmic resistivity $\rho_\parallel \equiv 2a_0 L R_3(R_0, H_0, L)$, where a_0 is the size of a single DCE. These values, as well as the Hall coefficient $R_H \equiv 2a_0 L R_1(R_0, H_0, L) H(R_0, H_0, L)/H_0$, have the following scaling behavior as functions of L:

$$\rho_\perp(R_0, H_0, L) = \rho_\parallel(R_0, H_0, L) = 2R_0 a_0 L^{\tilde{t}},$$

$$\tilde{t} = \frac{\ln 3}{\ln 2} \approx 1.585, \tag{9}$$

$$R_H(R_0, H_0, L) = 2R_0 a_0 L^{\tilde{g}},$$

$$\tilde{g} = \frac{\ln(3/2)}{\ln 2} \approx 0.585. \quad (10)$$

The value of $\tilde{t}$ is the same as that found in Ref. 22 for the zero field case, but the value of $\tilde{g}$ is new, and may be compared to the value found in simulations, namely, $\tilde{g} \approx 0.42$.[7]

From (6)–(8) it is clear that the values $H = \infty$, $\gamma = \sqrt{2}$ also constitute a fixed point of the transformation. For $|H_0| \gg 1$, the transverse and longitudinal ohmic resistivities and the Hall coefficient have the following scaling behavior:

$$\rho_\perp(R_0, H_0, L) \propto \rho_\parallel(R_0, H_0, L) \propto a_0 R_0 L^{\tilde{t}_H},$$

$$\tilde{t}_H = \frac{\ln(\sqrt{2}+2)}{\ln 2} \approx 1.772, \quad (11)$$

$$\rho_\perp(R_0, H_0, L)/\rho_\parallel(R_0, H_0, L) = \sqrt{2}, \quad (12)$$

$$R_H(R_0, H_0, L) \propto a_0 R_0 L^{\tilde{g}_H}, \quad \tilde{g}_H = 1. \quad (13)$$

These results may be compared with those of Ref. 18, namely $\tilde{t}_H \approx 2.669$, $\tilde{g}_H \approx 0.927$, which were obtained for a percolating network model from an approximate real-space renormalization-group transformation.

Suppose we start with $H_0 \gg 1$. From (7) and (8) it follows that in this case $H(n+1) = \frac{2}{\sqrt{2}+2} H(n)$. Since H keeps decreasing with each iteration of the gasket, i.e.,

$$H(R_0, H_0, L) = H_0 L^{\ln \frac{2}{\sqrt{2}+2}/\ln 2} \equiv H_0 L^{1-\tilde{t}_H},$$

therefore even if we start with $H_0 \gg 1$, we always eventually cross over to the weak-field regime $H \ll 1$, in which the behavior is dominated by the $H_0 = 0$ fixed point. This occurs when $L = H_0^{1/(\tilde{t}_H - 1)}$, which defines a (magnetic) field-dependent length ξ_H, which for this model is equal to $H_0^{\nu_H}$, $\nu_H = \frac{1}{\tilde{t}_H - 1} \approx 1.296$. This magnetic correlation length has a finite value as long as the field is finite. For $H_0 > 2$, the dependence of $\rho_\perp(R_0, H_0, L)/H_0$ on L and H_0 is very well described by a scaling function of the single variable L/ξ_H—see Fig. 5.

We would like to point out that the characteristic length ξ_H is related only to the distribution of the macroscopic currents in the system. It is therefore not directly comparable to any of the physical microscopic lengths such as cyclotron radius or mean free path. In particular, even though in a free-electron metal the parameter H_0 is essentially equal to the ratio of mean free path to cyclotron radius and $\xi_H = a_0 H_0^{\nu_H}$, the basic length scale a_0 is not related to any microscopic length scale. It is in fact determined simply by the size of the DCE in the case of the network models, and by the actual sizes of the metallic grains in a real metal-nonmetal composite.

The detailed local current distribution in the 3D gasket is obtained as a by-product of the exact solution of

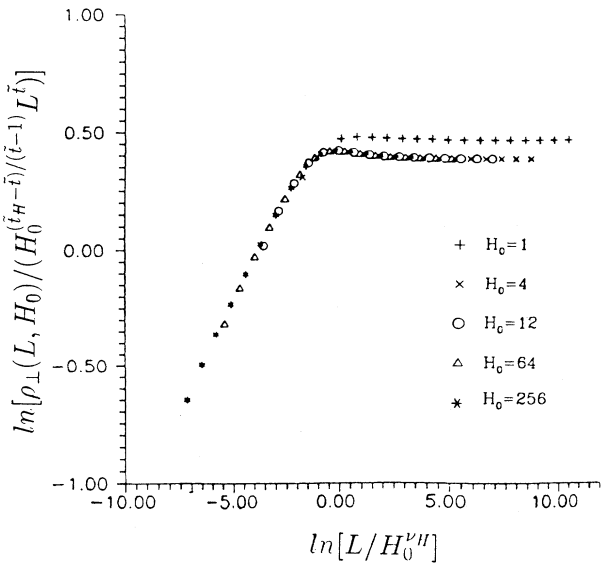

FIG. 5. log-log plot of the normalized ohmic resistivity $\rho_\perp(L, H_0)/[H_0^{(\tilde{t}_H-\tilde{t})/(\tilde{t}_H-1)}\rho(L,0)]$ vs L/ξ_H for the 3D Sierpinski-gasket model. The values of L go up to 32 768, while the values of H_0, measured in units of the Hall to ohmic resistivity ratio ρ_H/ρ, go up to 256.

Kirchhoff's equations: On a scale $L \ll \xi_H$ it is found that $i_1/i_2 \sim 1/H_0^2$, while on a scale $L \gg \xi_H$ it is found that $i_1/i_2 = \mathcal{O}(1)$ (see Fig. 4 for the definition of the local currents i_1, i_2, i_x). In the latter case the local currents are the same as when $H_0 = 0$. The loop current i_x attains its maximum value when $L \approx \xi_H$.

The critical exponents $\tilde{t}$, $\tilde{g}$ obtained from the 3D Sierpinski gasket for the weak- (magnetic) field regime may be compared with values obtained for these exponents in percolating network models (see Refs. 21 and 7, and references therein). The values are similar but different, which confirms the generally accepted belief that the gasket is not a good quantitative model for the percolating backbone but leads to a reasonable qualitative picture. In the next section we will see that in the strong field regime, the discrepancies are much greater. Nevertheless the scaling properties of the high-field magnetotransport obtained for the Sierpinski gasket still hold true for a real percolating system.

IV. MONTE CARLO SIMULATION OF PERCOLATING NETWORKS IN A STRONG MAGNETIC FIELD

There exist essentially two different approaches to solving a 3D random-resistor network near the percolation threshold in order to evaluate the macroscopic transport properties, namely, relaxation methods[24,25] and transfer matrix methods.[26,7] Both of these have one or more drawbacks in the context of our problem. The relaxation methods are very inefficient at coping with the strong, far-reaching distortions of the current and voltage dis-

tributions caused by a strong magnetic field, since these phenomena drastically slow down the rate of relaxation. In the transfer matrix method there is no question of relaxation, but one is tied down to a restricted set of boundary conditions which create severe problems in the interpretation of the results (see the Appendix for a discussion of this). We therefore used an extension of the method of Refs. 27 and 28.

The first step is to set up a 3D, simple cubic, independent random site lattice, and identify the percolation cluster. Each site of this cluster is occupied by an identical, six-terminal DCE of the type described in Sec. II, which is characterized by a 6×6 conductance matrix $\hat{G} = \hat{R}^{-1}$. Due to the fractal nature of the percolation cluster many internal terminals (i.e., terminals not at the top or bottom layer of the sample) are unconnected and thus no current can flow into them. At this stage, all such terminals are eliminated, and the matrices $\hat{G}$ of the relevant DCE's are appropriately transformed into smaller matrices. Next, we eliminate all dangling DCE's, namely those that have only one (connected) terminal. These two steps are iterated until every remaining internal DCE (i.e., one that does not have a terminal in the top or bottom layer) has at least two (connected) terminals. At this stage, connected pairs of DCE's are combined to form single DCE's (see Fig. 6). Sometimes the combined DCE has an increased number of terminals, and its conductance matrix then has a correspondingly increased number of rows and columns. This procedure is repeated so as to gradually reduce the total number of DCE's, at the expense of an increased number of terminals for individual DCE's. We do not attempt to combine two DCE's if the resultant DCE has more than 50 terminals. If the original network was sufficiently close to the percolation threshold, then the percolation cluster is sufficiently ramified so that the number of terminals per DCE does not increase too quickly. We are finally left with a number of multiterminal DCE's that are interconnected, and for which Kirchhoff's equations must be solved by brute force at all the internal terminals. Most of the remaining terminals are however at the top or bottom layers, so that the total

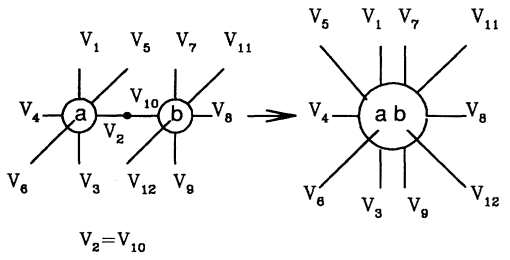

FIG. 6. Illustration of the coupling procedure of two connected DCE's, in which two six-terminal DCE's, connected at one of their terminals, are replaced by a single DCE with 10 terminals. At the percolation threshold, the fraction of terminals that are connected is so small that the actual number of terminals per DCE that one has to cope with when this procedure is iterated is never very large. In that case, when the system has only four external terminals, the coupling procedure can be iterated to its conclusion, at which point we are left with a single, four-terminal DCE.

number of equations that must be solved simultaneously is rather modest. For example, in all the networks we simulated at p_c that were smaller than $25 \times 25 \times 25$ this procedure led to only a single resultant DCE, and thus all effective parameters were obtained immediately. For larger systems, the number of equations that remain to be solved at the end of the procedure increases approximately as L^2, where L is the linear size. This behavior is in agreement with the fractal dimension of the 3D percolation backbone which is known to be close to 2.[21] Thus for a random network of size $100 \times 100 \times 100$ the typical number of these equations does not exceed about 40. These equations were solved by Gauss-Jordan elimination, taking a few seconds on a Sun Sparc1 workstation. Most of the computing time is spent on the reduction of the original network to this final system of equations. Since the number of DCE's is reduced by one at each step of the reduction process, the total number of operations $\mathcal{N}$ is proportional to the size of the backbone L^{d_f}. One can compare this estimate with $\mathcal{N} \propto L^7$ for the transfer matrix method and $\mathcal{N} \propto L^4$ for the relaxation method. Moreover, the appearance of strong Hall fields makes the relaxation method very unstable: we were unable to make it converge when $H_0 > 20$. Therefore the method described above is not only very efficient, but seems to be the only known numerical method able to solve such problems. A detailed analysis of this method will be presented elsewhere.[29]

In order to obtain results for the macroscopic magnetotransport, we must apply appropriate boundary conditions to the $L \times L \times L$ network. This is done by prescribing

$$V_{\rm bot}(i,1,k) = iE_0 \sin\theta + V_0, \tag{14}$$

$$V_{\rm top}(i,L,k) = iE_0 \sin\theta + LE_0 \cos\theta + V_0, \tag{15}$$

at the terminals on the bottom and top layers, respectively. Here V_0 is an arbitrary constant. This is equivalent to applying an average electric field of magnitude E_0 in the x,y plane, at an angle θ with respect to the y axis. The total current in the y direction is calculated, and used to express the current density j_y in that direction. As function of E_0, θ it has the following form:

$$j_y = AE_0 \cos\theta + BE_0 \sin\theta. \tag{16}$$

The coefficients A, B are determined for each realization of the network and then averaged over the different realizations. At the angle $\theta_{\max}$, for which the averaged current density $\langle j_y \rangle$ is maximal, the electric field components $E_0 \cos\theta_{\max}$, $E_0 \sin\theta_{\max}$ are taken to be the ohmic and the Hall fields, respectively. The bulk effective ohmic and Hall resistivities $\rho^{(e)}$, $\rho_H^{(e)}$ are therefore given by

$$\rho^{(e)} = \frac{\langle A \rangle}{\langle A \rangle^2 + \langle B \rangle^2}, \tag{17}$$

$$\rho_H^{(e)} = \frac{\langle B \rangle}{\langle A \rangle^2 + \langle B \rangle^2}. \tag{18}$$

Since the linear size L of the networks we simulated was never greater than 63, boundary or surface effects need to

be discussed. At p_c, the percolating cluster includes loops and blobs on all scales, including the smallest ones.[21] Therefore a boundary with a prescribed, uniformly varying set of potentials as described above will short out or otherwise drastically alter any of those loops that it happens to cut through (see Fig. 7). In the Appendix we show that this can change the measured magnetotransport coefficients considerably and thus easily obscure the bulk behavior of the system at the small sizes that were simulated. In order to avoid this pitfall, we applied the above-mentioned boundary conditions only to one pair of terminals at the top layer and one pair of terminals at the bottom layer of the network, always choosing the pair of terminals with the largest chemical distance between its members. The other surface terminals were left unconnected, with zero current flowing to them. Our system is therefore really a large four-terminal device, similar to the elementary DCE but with fewer terminals.

All the simulations reported here were done using networks at $p = p_c \approx 0.3116$ (see Ref. 21). We averaged the results over 1000 realizations for each of the system sizes $L = 2, 4, 6, 9, 13, 19, 28, 42, 63$ and for each of the dimensionless magnetic field values $H = 0.5, 1, 2, 4, ..., 32\,768$. The effective ohmic resistivity $\rho^{(e)}(L, H)$, obtained in this way from Eq. (17), is shown in Figs. 8 and 9. For $H = 0$, the ohmic resistivity results

$$\rho^{(e)}(L, 0) \sim L^{\tilde{t}}, \quad \tilde{t} = 2.2 \pm 0.1, \tag{19}$$

are in good agreement with known results (see Ref. 30 and references therein). For intermediate values of H, namely $1 \ll |H| \ll L$, the behavior of the ohmic resistivity $\rho^{(e)}(L, H)$ is in qualitative agreement with EMT: The difference $\rho^{(e)}(L, H) - \rho^{(e)}(L, 0)$ is proportional to H and tends to zero with increasing L. The situation is quite different in the case of strong magnetic field, i.e., when $H \gg L$. As H tends to infinity, the effective ohmic resistivity $\rho^{(e)}(L, H)$ saturates but depends strongly on the system size L:

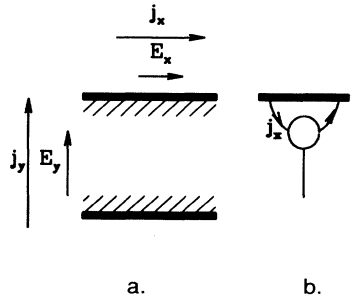

FIG. 7. (a) A schematic representation of the surface layers with enhanced conductivity. The effective conductivity of the surface layers remains unchanged when the concentration p approaches p_c. (b) An example of a surface DCE with two of its terminals shorted by the boundary. When an electric field is applied in the x direction, j_x is mainly determined by such surface DCE's.

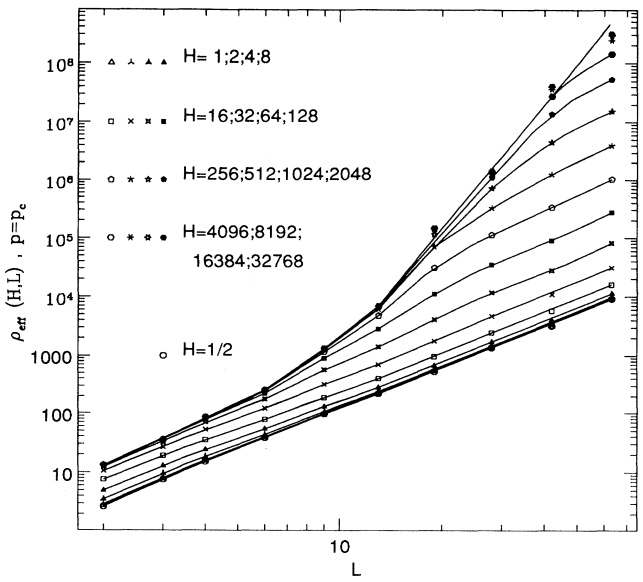

FIG. 8. Results from Monte Carlo (MC) simulations for the bulk effective ohmic resistivity $\rho^{(e)}(L, H)$ at the percolation threshold $p_c = 0.3116$ as function of the system size L for different values of $H \equiv \rho_H/\rho$ from $H = 0.5$ up to $H = 32\,768$. The full curves were obtained by fitting a natural cubic spline to points with the same H. For a fixed size L, $\rho^{(e)}(L, H)$ saturates as $H \to \infty$.

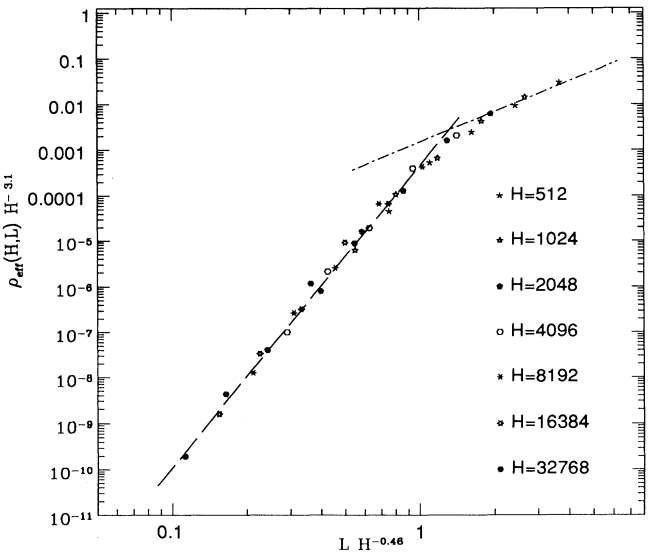

FIG. 9. Scaling behavior of the effective ohmic resistivity $\rho^{(e)}(L, H) = H^{\tilde{t}_H \nu_H} f(L/\xi_H)$, where $\xi_H = H^{\nu_H}$ is the magnetic correlation length, $\nu_H \approx 0.46$, and $\tilde{t}_H \nu_H \approx 3.1$. Dashed lines correspond to the asymptotic behavior at strong fields $\rho^{(e)}(L, H) \sim L^{\tilde{t}_H}$, $\tilde{t}_H \approx 6.7$ and at weak fields $\rho^{(e)}(L, H) \sim L^{\tilde{t}}$, $\tilde{t} \approx 2.2$. The crossover occurs when $L/\xi_H \approx 1$.

$$\rho^{(e)}(L,H) \sim L^{\tilde{t}_H}, \quad \tilde{t}_H = 6.7 \pm 0.5. \tag{20}$$

This behavior is only evident for $L > 10$. This can be understood if we suppose that the self-similar nature of the percolation cluster becomes fully developed only when $L > 10$. One can also compare this result with the distribution $f(\mathcal{L})$ of the lengths $\mathcal{L}$ of singly connected links in the percolation cluster.[31] This distribution has the form $f(\mathcal{L}) = A\mathcal{L}^{1.3}\exp(-\mathcal{L}/\mathcal{L}_0)$, where the characteristic length $\mathcal{L}_0$ is about 9. This means that the number of singly connected spanning channels drops to zero very rapidly when $\mathcal{L} > 9$.

The qualitative picture of high-field magnetoresistance that emerges from the simulations is similar to the one found from the Sierpinski-gasket model in Sec. III, and from our preliminary study using an approximate real-space renormalization-group:[18] The ohmic resistivity $\rho^{(e)}(L,H)$ is a scaling function of the ratio L/ξ_H (see Fig. 9)

$$\rho^{(e)}(L,H) = H^{\tilde{t}_H\nu_H} f(L/\xi_H), \tag{21}$$

where $\xi_H = H^{\nu_H}$ is the magnetic correlation length, and $\nu_H = 0.46 \pm 0.2$ and $\tilde{t}_H\nu_H \approx 3.1$ are new critical exponents. When L increases, the ratio $\rho^{(e)}(L,H)/H^{\tilde{t}_H\nu_H}$ first increases according to Eq. (20). But when $L > \xi_H$, a crossover occurs to an increase that is described by Eq. (19).

Using finite size scaling arguments,[21] it is possible to conclude that in an infinitely large system at $p \neq p_c$, $\rho^{(e)}(p,H)$ will exhibit the following type of scaling behavior:

$$\rho^{(e)}(p,H) = H^{\tilde{t}_H\nu_H} f(\xi_p/\xi_H), \tag{22}$$

where $\xi_p = [(p-p_c)/p_c]^{-\nu}$ is the percolation correlation length—the typical scale of geometrical inhomogeneity in the percolation cluster. From our results we conclude that this equation should hold when p is close to p_c and $H > 500$. In a system of this type, the formally calculated magnetic correlation length ξ_H can turn out to be larger than the percolation correlation length ξ_p. This means that the spatial scale of current and voltage fluctuations can be larger than ξ_p. This expectation is confirmed by the form of the distribution function of ohmic resistivities $f(\rho)$ for different realizations of the system (see Fig. 10). This function has three peaks, the lowest at ρ_{01}, whose position saturates as $H \to \infty$, a second at ρ_{02}, whose position keeps increasing as H^2, and a third at $\rho_{03} = \infty$ (not shown). This form of $f(\rho)$ is similar to the distribution function expected for a three-component percolating system without any magnetic field, with resistivities satisfying $\rho_{02} \gg \rho_{01}$ and $\rho_{03} = \infty$. In such a system we expect that the spatial size of the current and voltage fluctuations will sometimes be much larger than the percolation correlation length ξ_p. The three-peak character of the distribution function $f(\rho)$ leads to some uncertainty in determining the effective parameters, and clearly deserves to be studied further.

The Hall coefficient $R_H^{(e)}(L,H) = \rho_H^{(e)}(L,H)/H$ is shown in Figs. 11 and 12 as function of the dimensionless magnetic field H and system size L. Although the accuracy achieved for $R_H^{(e)}(L,H)$ is less than that which was possible for the ohmic resistivity, it is nevertheless possible to draw some conclusions. At small H the Hall coefficient satisfies $R_H^{(e)} \sim L^{\tilde{g}}$, where the value of the critical exponent $\tilde{g} = 0.8 \pm 0.2$ is somewhat larger than

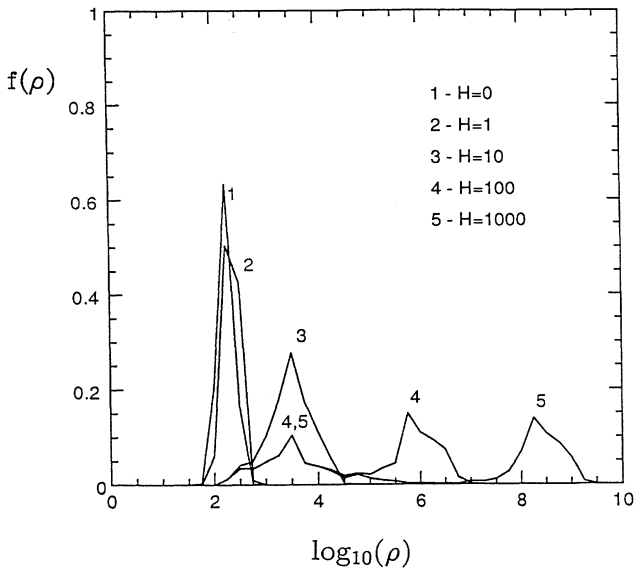

FIG. 10. Distribution functions $f(\rho)$ for ohmic resistivities of different realizations of the system at size $L = 13$ and magnetic field strengths $H = 0, 1, 10, 100, 1000$.

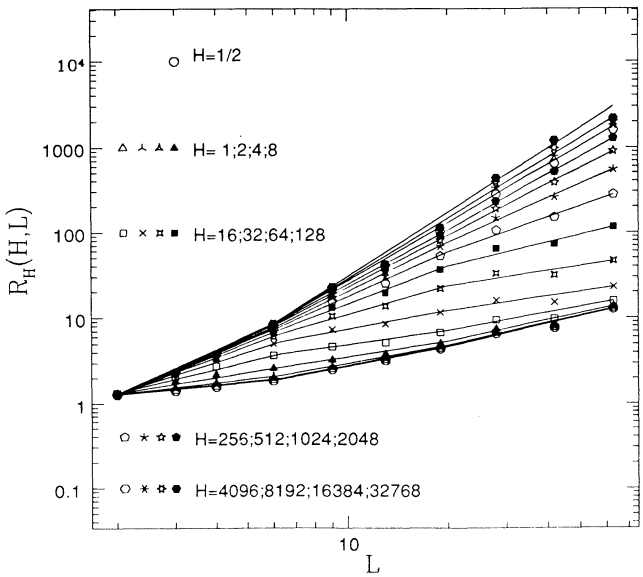

FIG. 11. Results from MC simulations for the bulk effective Hall coefficient $R_H^{(e)}(L,H)$ at the percolation threshold $p_c = 0.3116$ as function of the system size L for different values of $H \equiv \rho_H/\rho$ from $H = 0.5$ up to $H = 32\,768$. The full curves were obtained by fitting a natural cubic spline to points with the same H. For a fixed size L, $R_H^{(e)}(L,H)$ saturates as $H \to \infty$.

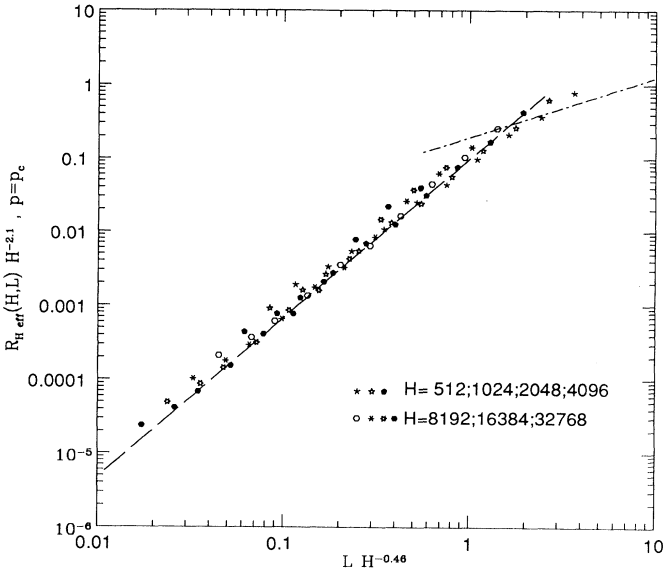

FIG. 12. Scaling behavior of the effective Hall coefficient $R_H^{(e)}(L,H) = H^{\tilde{g}_H \nu_H} f(L/\xi_H)$, where $\xi_H = H^{\nu_H}$ is the magnetic correlation length, $\nu_H \approx 0.46$, and $\tilde{g}_H \nu_H \approx 2.1$. The dashed lines correspond to the asymptotic behavior at strong fields $R_H^{(e)}(L,H) \sim L^{\tilde{g}_H}$, $\tilde{g}_H \approx 4.5$ and at weak fields $R_H^{(e)}(L,H) \sim L^{\tilde{g}}$, $\tilde{g} \approx 0.8$. The crossover occurs when $L/\xi_H \approx 1$.

the value $\tilde{g} \approx 0.42$ found in Ref. 7. We believe that the method used to calculate the low-field Hall resistivity in that reference is the most accurate one, since it is based on a simulation of random-resistor networks at $H = 0$ and does not depend on evaluating the small difference between the behavior at $H = 0$ and at a small but nonzero H. In the work of Straley (Ref. 9) an approach similar to ours was used but with different boundary conditions and it was then found that $\tilde{g} \approx 0$. The size of the systems considered in Ref. 9 was rather small $L \leq 20$, and the final result for $\tilde{g}$ was obtained as the difference between two large exponents for ohmic and Hall conductivities. Conflicting results for $\tilde{g}$ were also obtained in another calculation.[32] We believe that it will be necessary to increase the system size and the number of realizations and also to carefully consider the effect of the boundary conditions in order to resolve these discrepancies and determine the accurate value of $\tilde{g}$.

At intermediate values of H, $R_H^{(e)}$ depends on H, but when H tends to infinity, it again becomes independent of H. It then increases as $R_H^{(e)} \sim L^{\tilde{g}_H}$, where the strong-field critical exponent $\tilde{g}_H$ is estimated to be $\tilde{g}_H = 4.5 \pm 1.0$. The Hall coefficient is a scaling function of L/ξ_H in the same region of L and H as was the ohmic resistivity (see Fig. 12):

$$R_H^{(e)}(L,H) = H^{\tilde{g}_H \nu_H} f(L/\xi_H). \tag{23}$$

Finite size scaling arguments again allow us to write a scaling form for $R_H^{(e)}(p,H)$ in the case of an infinitely large system at $p \neq p_c$

$$R_H^{(e)}(p,H) = H^{\tilde{g}_H \nu_H} f(\xi_p/\xi_H). \tag{24}$$

V. SUMMARY AND DISCUSSION

We have carried out an elaborate theoretical and numerical study of magnetotransport in percolating composites. We proposed a discrete model (i.e., a discrete circuit element or DCE) for magnetotransport and showed that, when used in an appropriate network model, it has the ability to reproduce faithfully some important properties of a continuum percolating medium. In order to study the effective ohmic resistivity and Hall coefficient of such a system in the presence of a magnetic field we solved exactly a 3D Sierpinski-gasket fractal network of such elements and also simulated random networks of such elements. The simulations employed a new and very efficient algorithm which should also be useful for other problems. Our main result is the qualitative observation that, in contrast with previous results obtained from effective medium theory (EMT) but in agreement with our own earlier and preliminary study, there is a large magnetoresistance in the vicinity of the percolation threshold. In the strong-field limit the ohmic resistivity and Hall coefficient do not depend on the value of the magnetic field but their critical behavior near the percolation threshold is characterized by new critical exponents $\tilde{t}_H$ and $\tilde{g}_H$, respectively. We obtained values for these new exponents, but those values need to be calculated more accurately in future work. We introduced a new physical parameter, the magnetic correlation length ξ_H, which depends on the value of the dimensionless magnetic field $H = \omega_L \tau$ as H^{ν_H}, with the (new) critical exponent $\nu_H = 0.45 \pm 0.10$. Both the ohmic resistivity and the Hall coefficient are scaling functions of the ratio ξ_p/ξ_H, where ξ_p is the percolation correlation length, and those functions are determined from the simulations. It is shown that the behavior of the ohmic resistivity in the presence of a strong magnetic field depends on details of the structure of the percolation cluster. Consequently, we expect that experimental studies of magnetotransport in a composite medium can shed light on details of the internal microstructure. Although we have assumed in this paper that the conducting component was free-electron metal-like in that it had zero magnetoresistance, we believe that the behavior we found will continue to hold for all composites where the conducting component has its ohmic resistivity saturated in a strong magnetic field, and where the Hall resistivity remains proportional to the magnetic field at such field strengths. This encompasses the case of metals and uncompensated semiconductors with a closed Fermi surface. Presumably, our methods can be extended to calculate the magnetotransport also in composites with other types of components, including superconducting materials.

ACKNOWLEDGMENTS

This research was supported in part by the U.S.-Israel Binational Science Foundation under Grant No. 88-432,

by the Basic Research Fund of the Israel Academy of Sciences and Humanities under Grant No. 212/921, by the Sackler Institute for Theoretical Physics at Tel Aviv University, and by a grant from the Bureau for Absorption in Science.

APPENDIX

First we present some details of the exact solution of the 3D Sierpinski gasket with one four-terminal DCE at each vertex. When four such DCE's are interconnected as shown in Fig. 4, one obtains the first generation fractal which is also a four-terminal device. Its analysis is most easily accomplished by using the form of (4) for the resistance matrix $\hat{R}$. But for the first generation fractal, as well as for subsequent generation fractals, the resistance along the magnetic field is different from that in the transverse direction. It is easy to verify that such an anisotropic DCE is described by a resistance matrix of the following form:

$$\hat{R} = \frac{R_3}{2}\left[\begin{pmatrix} 1+\gamma & 0 & 1-\gamma & 0 \\ 0 & 1+\gamma & 0 & 1-\gamma \\ 1-\gamma & 0 & 1+\gamma & 0 \\ 0 & 1-\gamma & 0 & 1+\gamma \end{pmatrix} + H\begin{pmatrix} 0 & -1 & 0 & 1 \\ 1 & 0 & -1 & 0 \\ 0 & 1 & 0 & -1 \\ -1 & 0 & 1 & 0 \end{pmatrix}\right]. \tag{A1}$$

Suppose that a current i flows in the y direction going into terminal 3 of a DCE characterized by (A1) and leaving it by terminal 1 (see Fig. 4). The current vector, which describes the currents flowing out of the four terminals, then has the form $\mathbf{i} = \{i, 0, -i, 0\}$. Applying $\hat{R}$ of (A1) to this vector we get for the potential vector $\mathbf{V} = \{R_3\gamma i, R_3 H i, -R_3\gamma i, -R_3 H i\}$, which describes the potentials at the same four terminals. Now suppose that a current i flows in the x direction going into terminal 4 and out of terminal 2. The current vector is then $\mathbf{i} = \{0, i, 0, -i\}$, and the corresponding potential vector is $\mathbf{V} = \{-R_3 H i, R_3\gamma i, R_3 H i, -R_3\gamma i\}$. Finally, suppose that a current i flows through a DCE in the direction of the magnetic field. The current vector then has the form $\mathbf{i} = \frac{1}{2}\{i, -i, i, -i\}$, and the corresponding potential vector is $\mathbf{V} = \frac{1}{2}\{R_3 i, -R_3 i, R_3 i, -R_3 i\}$. Thus the matrix (A1) describes a DCE with a longitudinal resistance $2R_3$ that is different from the transverse resistance $2R_1 = 2\gamma R_3$. If we assign the linear size a_0 to a single DCE, it is easy to recognize that the matrix (A1) describes a material with the resistivity tensor:

$$\hat{\rho} = \begin{pmatrix} \rho_{\parallel} & -\rho_H & 0 \\ \rho_H & \rho_{\parallel} & 0 \\ 0 & 0 & \rho_{\perp} \end{pmatrix} = 2a_0 R_3 \begin{pmatrix} \gamma & -H & 0 \\ H & \gamma & 0 \\ 0 & 0 & 1 \end{pmatrix}. \tag{A2}$$

We now calculate the parameters of a four-terminal device composed of the four DCE's with resistance matrix (A1), as shown in Fig. 4. In order to calculate the new transverse resistance R_1' suppose that a current $i_1 + 2i_2$ enters terminal III (see Fig. 4) and exits from terminal I. In principle there are four independent loops in the circuit and therefore four independent currents and four Kirchhoff equations for the loop emf's. Due to symmetry, this number is reduced to three independent currents and three independent equations. The choice of currents is rather arbitrary. One convenient scheme is to consider all internal currents as composed of the currents i_1, i_2, and i_x as shown in Fig. 4. The potential at each terminal of the basic DCE's A, B, C, and D can be expressed in terms of these currents. For example, the potentials at the terminals of A are given by

$$\begin{aligned} V_1 &= R_3[\gamma i_1 + (1+\gamma) i_2 + H i_x], \\ V_2 &= R_3[-\gamma i_x - i_2 + H(i_1 + i_2)], \\ V_3 &= R_3[-\gamma i_1 + (1-\gamma) i_2 - H i_x], \\ V_4 &= R_3[\gamma i_x - i_2 - H(i_1 + i_2)]. \end{aligned}$$

In order to write Kirchhoff's equations we only need to know the voltage differences between different terminals of the same DCE. Those differences are independent of the particular gauge or offset, which in (A1) is chosen so as to make the sum of potentials at all terminals of a single DCE vanish. In this way we obtain

$$4\gamma i_1 + 4\gamma i_2 + 4H i_x = U_0/R_3, \tag{A3}$$

$$2\gamma i_1 + 4(\gamma+1) i_2 = U_0/R_3, \tag{A4}$$

$$2(\gamma+1) i_x - H i_1 = 0, \tag{A5}$$

Eq. (A3) was obtained by equating the external voltage U_0 the sum of the voltage $V_{A\,13}$ between terminals 1 and 3 of A and the voltage $V_{C\,13}$ between terminals 1 and 3 of C. Equation (A4) was obtained by equating U_0 to the sum of $V_{A\,12}$, $V_{B\,13}$, and $V_{C\,23}$. Equation (A5) was obtained by equating to zero the sum of $V_{A\,42}$, $V_{B\,14}$, and $V_{D\,21}$.

From the solution of these equations one can also calculate the Hall voltage drop V_0 between the external terminals II and IV. The new effective parameters R_1' and H' are given by

$$R_1' = \gamma' R_3' = \frac{(\gamma+1)[\gamma(\gamma+2) + H^2]}{(\gamma+1)^2 + H^2} R_3, \tag{A6}$$

$$H' = 2\frac{\gamma(\gamma+2) + H^2}{(\gamma+1)[\gamma(\gamma+1) + H^2]} H. \tag{A7}$$

To determine the effective longitudinal resistance it is necessary to calculate the voltage drop U_0 between, for example, terminals I and II when currents i flow into terminals II , IV and out of terminals I, III. It is possible to verify that in this case there are no currents flowing from A to C or from B to D. We thus obtain $U_0 = iR_3(2+\gamma)$, and consequently the following expression for the new longitudinal resistance:

$$R_3' = R_3 \frac{2+\gamma}{2}. \tag{A8}$$

The relations (A6)–(A8) immediately lead to the exact renormalization-group transformation (6)–(8).

We now consider in more detail the effect of the thin surface layers of percolating material that are adjacent to the boundaries where the electric potential is prescribed. Due to the electric shorting out of loops and blobs that intersect those boundaries, the effective conductivity of the adjacent layers is greatly enhanced compared to the bulk value at strong magnetic fields [see Fig. 7(a)]. Clusters (e.g., loops) of small size and with closely spaced multiple connections to the boundary are the most drastically affected by this. Since the percolating cluster has a self-similar structure,[21] the number and shape of these small clusters does not change when $p \to p_c$. Therefore the effective thickness l of those layers is of the order of the linear size of a unit cell of the network, i.e., 1. By a similar logic, the effective ohmic and Hall resistivities of these layers ρ_l, ρ_{Hl} remain of the same order of magnitude as those of the pure conducting component ρ, ρ_H even when $p \to p_c$. We now estimate the effect of those (two) layers by considering the entire system to be made of a thickness L of bulk material in series with a thickness $2l$ of the "surface layer material" described above. This leads to the following result for the y component of the current density:

$$j_y = \frac{E_0 \sin\theta}{\langle\langle\rho\rangle\rangle + \langle\langle\rho H^2\rangle\rangle} + \frac{\langle\langle H\rangle\rangle E_0 \cos\theta}{\langle\langle\rho\rangle\rangle + \langle\langle\rho H^2\rangle\rangle}, \tag{A9}$$

where the quantities

$$\langle\langle\rho\rangle\rangle = \rho_l \frac{2l}{L} + \rho^{(e)} \frac{L-2l}{L}, \tag{A10}$$

$$\langle\langle H\rangle\rangle = \frac{\rho_{Hl}}{\rho_l}\frac{2l}{L} + \frac{\rho_H^{(e)}}{\rho^{(e)}}\frac{L-2l}{L}, \tag{A11}$$

$$\langle\langle\rho H^2\rangle\rangle = \frac{\rho_{Hl}^2}{\rho_l}\frac{2l}{L} + \frac{\rho_H^{(e)\,2}}{\rho^{(e)}}\frac{L-2l}{L}, \tag{A12}$$

are simply volume averages in this three-layer system. Using the critical exponents $\tilde{t}$, $\tilde{g}$ we can now estimate these quantities for a system at the percolation threshold and in a weak magnetic field. We thus get

$$\langle\langle\rho\rangle\rangle \approx \rho_l \frac{2l}{L} + aL^{\tilde{t}}, \tag{A13}$$

$$\langle\langle H\rangle\rangle \approx \frac{\rho_{Hl}}{\rho_l}\frac{2l}{L} + bL^{-\tilde{t}+\tilde{g}}. \tag{A14}$$

From the values $\tilde{t} \approx 2.2$ and $\tilde{g} \approx 0.4$ we conclude that, when $L \to \infty$, the resistivity $\langle\langle\rho\rangle\rangle \sim L^{\tilde{t}}$, $\langle\langle H\rangle\rangle \sim 1/L$, and the Hall coefficient $R_H = \langle\langle H\rangle\rangle\langle\langle\rho\rangle\rangle/H_0 \sim L^{\tilde{t}-1} \approx L^{1.2}$. Thus the Hall coefficient is mostly determined by the surface layers and not by the bulk material.

* Permanent address.

[1] I. Webman, J. Jortner, and M.H. Cohen, Phys. Rev. B **15**, 1936 (1977).

[2] B.I. Shklovskii, Zh. Eksp. Teor. Fiz. **72**, 288 (1977) [Sov. Phys. JETP **45**, 152 (1977)].

[3] J.P. Straley, J. Phys. C **13**, 4335 (1980); **13**, L773 (1980).

[4] D.J. Bergman, Y. Kantor, D. Stroud, and I. Webman, Phys. Rev. Lett. **50**, 1512 (1983).

[5] D.J. Bergman, in *Annals of the Israel Physical Society*, edited by G. Deutscher, R. Zallen, and J. Adler (Hilger, London, 1983), Vol. 5, pp. 297–321.

[6] D.J. Bergman and D. Stroud, Phys. Rev. B **32**, 6097 (1985).

[7] D.J. Bergman, E. Duering, and M. Murat, J. Stat. Phys. **58**, 1 (1990), and references cited therein.

[8] A.S. Skal, J. Phys. C **20**, 245 (1987).

[9] J.P. Straley, Phys. Rev. B **38**, 11 639 (1988).

[10] C. Kittel, *Quantum Theory of Solids* (Wiley, New York, 1963).

[11] A.M. Dykhne, Zh. Eksp. Teor. Fiz. **59**, 641 (1970) [Sov. Phys. JETP **32**, 348 (1971)].

[12] K.S. Mendelson, J. Appl. Phys. **46**, 4740 (1975).

[13] B.Ya. Balagurov, Zh. Eksp. Teor. Fiz. **82**, 1333 (1982) [Sov. Phys. JETP **55**, 744 (1982)].

[14] D. Stroud and D.J. Bergman, Phys. Rev. B **30**, 447 (1984).

[15] B.Ya. Balagurov, Fiz. Tverd. Tela **28**, 3012 (1986) [Sov. Phys. Solid State **28**, 1694 (1986)].

[16] D. Stroud, Phys. Rev. B **12**, 3368 (1975).

[17] D. Stroud and F.P. Pan, Phys. Rev. B **13**, 1434 (1976).

[18] A.K. Sarychev, D.J. Bergman, and Y.M. Strelniker, Europhys. Lett. **21**, 851 (1993).

[19] H. Stachowiak, Physica **45**, 481 (1970).

[20] J.B. Sampsell and J.C. Garland, Phys. Rev. B **13**, 583 (1976).

[21] D. Stauffer and A. Aharony, *Introduction to Percolation Theory*, 2nd ed. (Taylor and Francis, Philadelphia, 1991).

[22] Y. Gefen, A. Aharony, B.B. Mandelbrot, and S. Kirkpatrick, Phys. Rev. Lett. **47**, 1771 (1981).

[23] D.J. Bergman and A.K. Sarychev, Physica A **191**, 470 (1992).

[24] I. Webman, J. Jortner, and M.H. Cohen, Phys. Rev. B **11**, 2885 (1975).

[25] G.G. Batrouni and A. Hansen, J. Stat. Phys. **52**, 747 (1988).

[26] B. Derrida and J. Vannimenus, J. Phys. A **15**, L557 (1982); H.J. Hermann, B. Derrida, and J. Vannimenus, Phys. Rev. B **30**, 4080 (1984).

[27] D.J. Frank and C.J. Lobb, Phys. Rev. B **37**, 302 (1988).

[28] A.P. Vinogradov and A.K. Sarychev, Zh. Eksp. Teor. Fiz. **85**, 1144 (1983) [Sov. Phys. JETP **58**, 665 (1983)].

[29] A.K. Sarychev (unpublished).

[30] A.K. Sarychev, A.P. Vinogradov, and A.M. Karimov, J. Phys. C **18**, L105 (1985).

[31] A.K. Sarychev, A.P. Vinogradov, and A.V. Goldenshtein, J. Phys. C **20**, L113 (1987).

[32] S. Marianer and D.J. Bergman, Phys. Rev. B **39**, 11 900 (1989).